Chemical Science

Accepted Manuscript

This article can be cited before page numbers have been issued, to do this please use: Y. zhuang, X. Liu, Y. Shen, Q. Wang, Z. Lin, Q. Zeng, X. Chen, L. Jiang, S. Yao and J. Ge, *Chem. Sci.*, 2026, DOI: 10.1039/D6SC01497F.

ROYAL SOCIETY OF CHEMISTRY

rsc.li/chemical-science

View Article Online
DOI: 10.1039/D6SC01497F

ARTICLE

Reversible One-Step Acylation Facilitates Mitochondrial Delivery of Functional RNA

Received 00th January 20xx,
Accepted 00th January 20xx

DOI: 10.1039/x0xx00000x

Yuli Zhuang,[a, †] Xia Liu,[b, †] Yuxuan Shen,[a] Qiuyue Wang,[a] Zhimin Lin,[a] Qian Zeng,[a] Xin Chen,[a] Linye Jiang,[a] Shao Q. Yao,[b] Jingyan Ge[a,*]

Abstract: Mitochondria-targeted RNA therapeutics hold promise for treating mitochondrial disorders and cancer, yet effective mito-chondrial gene modulation remains challenging due to the strong negative charge and intrinsic instability of RNA, which hinder transport across the mitochondrial double membrane. Herein, we demonstrate, for the first time, mitochondrial RNA delivery enabled by reversible 2'-hydroxyl (2'-OH) acylation chemistry. Installation of a triphenylphosphonium (TPP)-bearing acyl group at the RNA 2'-OH in a single step creates a plug-and-play platform that simultaneously enhances RNA stability and directs selective mitochondrial accumulation, while allowing spontaneous recovery of native RNA structure and activity. In cell-based assay, this strategy enables efficient and selective silencing of mitochondria-encoded genes with mini-mal off-target effects. Importantly, in vivo delivery of siND1 selectively suppresses MTND1 expression without affecting MTCO1 and significantly inhibits tumor growth in a xenograft model. Conclusively, this work establishes reversible RNA acylation as a simple and versatile chemical framework for mitochondrial RNA delivery and therapy.

Introduction

The mitochondrial genome (mtDNA) encodes essential components of the oxidative phosphorylation machinery and sustains autonomous transcription and translation within mitochondria. Consequently, mitochondrial gene expression is central to cellular energy metabolism and redox homeostasis.[1,2] Pathogenic mtDNA mutations underlie numerous severe diseases, and mitochondrial dysfunction is increasingly recognized as a hallmark of cancer.[3-6] These observations underscore a pressing need for strategies that enable precise and selective modulation of mitochondrial gene function.

Although RNA-based technologies such as RNAi, CRISPR, and mRNA therapeutics have transformed nuclear gene regulation,[7-9] progress in mitochondrial gene engineering has been markedly slower.[10-14] This limitation arises primarily from the impermeable double-membrane architecture of mitochondria and the intrinsic instability and polyanionic nature of RNA, which together severely restrict mitochondrial entry and persistence of exogenous RNAs. To address this challenge, mitochondrial delivery has been explored using ligands such as mitochondrial targeting sequence (MTS) peptides and lipophilic cations, most notably triphenylphosphonium (TPP).[15,16] These strategies rely on permanent attachment of mitochondria-targeting motifs to RNA,[17-21] which, despite enabling broadly applicable targeting, introduces irreversible structural perturbations that can interfere with native RNA folding, target recognition, and biological activity.[22-23] As a result, approaches that enable efficient mitochondrial RNA delivery while fully restoring the RNA to its unmodified, native state remain exceedingly limited.

In parallel, RNA instability remains a major challenge. While material-based carriers and permanent chemical modifications can improve RNA stability,[24-26] they often compromise biological compatibility and are poorly suited to mitochondrial systems with distinct transcriptional and translational machinery. Although vector-mediated delivery of unmodified RNA offers advantages, [27-29] yet the accumulation of delivery vehicles could burdens on mitochondrial homeostasis. Therefore, simple reversible RNA modification became emerged as an attractive chemical strategy.[30-35] In particular, pioneered by Kool group, transient 2'-hydroxyl acylation ("RNA cloaking") provides a simple and general means to enhance RNA stability while preserving the capacity for spontaneous recovery of native structure and function. Subsequent work by Zhu and coworkers introduced stimuli-responsive 2'-OH RNA "uncloaking" strategies that enable controlled intracellular release. Despite these advances, RNA cloaking has thus far been limited to global stabilization and intracellular activation, it has not yet been demonstrated as a strategy for targeted subcellular RNA delivery, particularly to mitochondria.

[a] State Key Laboratory of Green Chemical Synthesis and Conversion, Zhejiang Key Laboratory of Bioorganic Synthesis, Col-lege of Biotechnology and Bioengineering, Zhejiang University of Technology, Hangzhou 310014, China, E-mail: gejy@zjut.edu.cn
[b] Department of Chemistry, National University of Singapore, Singapore 117543
† These authors contributed equally to this work.

View Article Online
DOI: 10.1039/D6SC01497F

ARTICLE

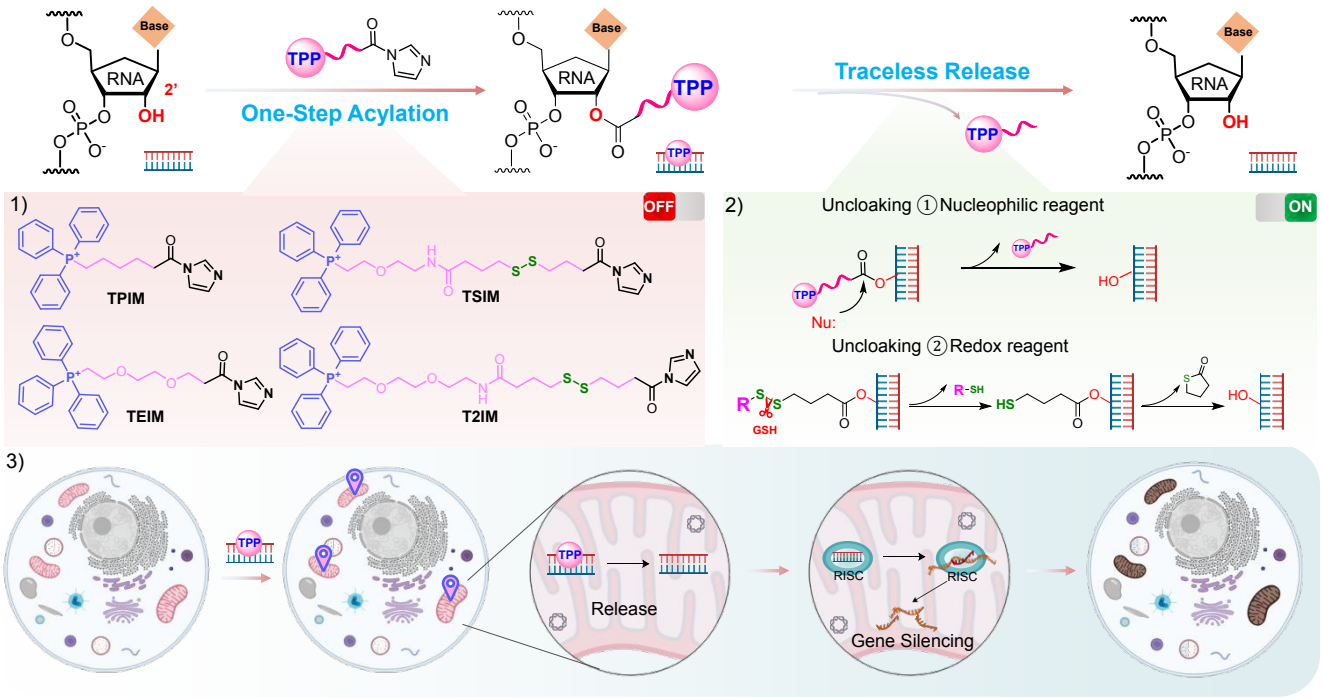

Figure 1. Scheme illustrating the key steps of mitochondria-targeted RNA delivery based on a TPP-conjugated acylimidazole reagent: 1) Chemical structures of the TPP-acylimidazole derivatives; 2) Activation ("uncloaking") and traceless release of the targeted RNA; 3) Mitochondria-specific delivery and subsequent gene-silencing function.

Herein we report the first example of mitochondrial RNA delivery enabled by reversible RNA cloaking. We describe a modular chemical strategy that integrates transient 2'-OH acylation with a mitochondria-directing TPP motif (Figure 1). This single-step modification simultaneously stabilizes RNA and enables its mitochondrial targeting, while preserving its ability to regain native structure and function upon intracellular traceless release. This plug-and-play platform eliminates the need for permanent peptide or linker conjugation and establishes reversible RNA acylation as a general chemical framework for mitochondrial RNA delivery and gene regulation.

Result and Discussion

Design, RNA modification, and reversible stabilization of IM@RNA

Four TPP-conjugated acylimidazole reagents (Figure 1) were rationally designed and synthesized to enable reversible covalent modification of RNA at the 2'-OH position. These reagents differ primarily in the length of the linker connecting the TPP moiety to the acylimidazole reactive center: (i) TPIM, featuring a long-chain aliphatic linker; (ii) TEIM, incorporating a flexible diethylene glycol linker; (iii) TSIM, containing a short PEG linker with a redox-responsive disulfide bond; and (iv) T2IM, combining a longer PEG linker with a disulfide unit. The detailed synthetic routes and structural characterization of the corresponding acid precursors are provided in the Supporting Information. All acylimidazole reagents were freshly generated in situ from their corresponding carboxylic acids *via* 1,1'-carbonyldiimidazole (CDI) activation and subsequently reacted with RNA under mild conditions to afford IM-modified RNA (IM@RNA).[33] This one-step cloaking process enables efficient esterification of accessible 2'-OH groups along the RNA backbone. Importantly, the reversibility of the modification is inherently engineered to linker chemistry: TPIM and TEIM rely on ester bond hydrolysis triggered by nucleophilic or mildly alkaline conditions, whereas TSIM and T2IM incorporate disulfide bonds that could undergo reductive cleavage in thiol-rich environments, such as those containing glutathione (GSH), ultimately leading a thermodynamically stable five-membered ring formation to traceless release of native RNA (Figure 1).[34]

We selected siRNA (~20 bp) as a model substrate to optimize the cloaking conditions. Based on reports, five acylimidazole reagents-including a previously described but non-targeted control reagent, CDI-activated *N*,*N*-dimethylglycine (DGIM, Figure 2A)-were incubated with siRNA in a DMSO/water mixture (1:4, v/v) at room temperature for 4 h with gentle agitation.[33]

View Article Online
DOI: 10.1039/D6SC04197F

The amounts of all these reagents were in large excess relative to that of the RNA. The modified RNAs were purified by ethanol precipitation to afford the acylated products, termed IM@RNA. Concentration-dependent acylation was first evaluated by agarose gel electrophoretic mobility shift assays. As shown in Figures S1, all reagents induced clear mobility shifts of siRNA, confirming successful acylation. Notably, compared with DGIM, TPP-conjugated ones produced more pronounced smeared band shifts at lower concentrations, suggesting that the positively charged TPP moiety enhances acylation efficiency, likely through electrostatic interactions with RNA. Therefore, the TPP ones were applied at a concentration of 100 mM, approximately one-tenth that of DGIM, for the generation of IM@RNA (Figures 2B and S2). The MALDI-TOF MS data further demonstrates that different acylation reagents result in varying degrees of RNA modification (Figure 2C and Figure S3). Specifically: TPIM displayed the highest level of acylation, with an average modification of approximately 8 added acyl groups per strand (for strands > 18 nt). In contrast, TSIM and T2IM with disulfide bonds showed a noticeably lower degree of acylation. Furthermore, the data indicates that the specific length and conformation of the RNA (single-stranded versus double-stranded) also have a slight influence on the overall acylation levels.

For IM@RNA to function as a practical delivery and protection platform, the covalent modification must be reversible under intracellularly relevant conditions. Because IM@RNA is linked through ester bonds, deacylation can be triggered either by hydrolysis or by reductive cleavage of the linker, depending on reagent design. To evaluate reversibility, IM@RNA samples were incubated under mildly alkaline conditions (200 mM Tris buffer, pH 8.8) or in the presence of GSH (20 mM), followed by purification and agarose gel electrophoretic analysis. As shown in Figure 2D and Figure S4, all the complexes underwent efficient deprotected under alkaline or reductive environment. These results confirmed that both hydrolysis- and redox-triggered uncloaking pathways could enable efficient recovery of unmodified RNA, supporting the intracellular applicability of this platform.

We next investigated whether esterification of the 2'-OH group could confer protection against enzymatic degradation. Heat deanealing TPIM@siNC^{FAM} (fluorescent FAM moiety modified siNC) were incubated with RNase A (100 μg/mL) for 30 min and analyzed by agarose gel electrophoresis (Figure 2E). The PAGE results clearly demonstrate the heterogeneous protective effect of our modification against RNase A. Specifically, upon treatment with RNase A, the less-modified or uncloaked RNA populations are degraded, as shown by the attenuation of the lower bands. However, the populations with higher levels of modification (corresponding to the distinct upper bands) remain well-protected and retained. Therefore, this combination of reversibility and partial stability establishes IM@RNA as a robust chemical platform for subsequent mitochondrial delivery and functional studies

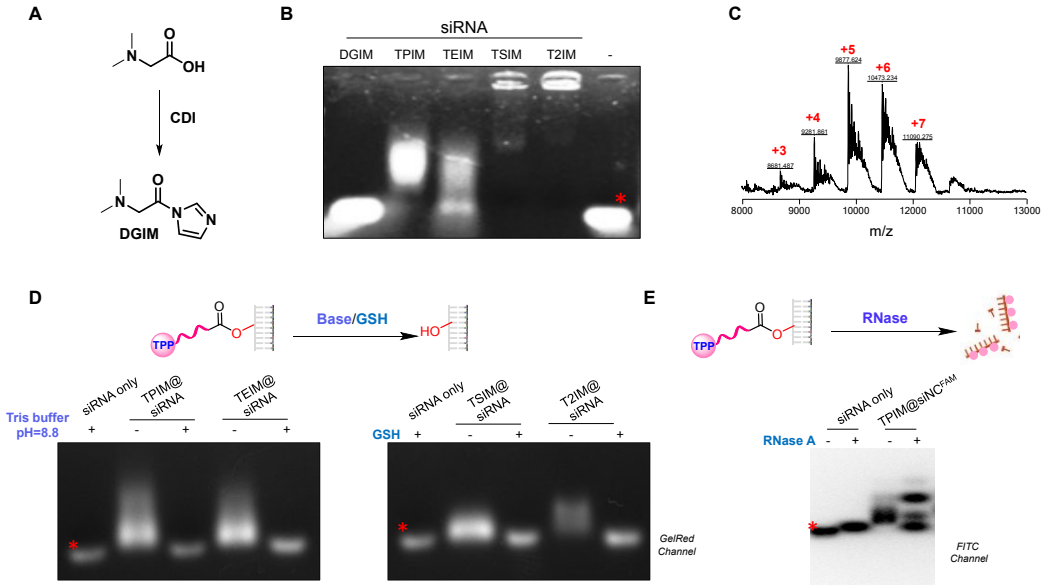

Figure 2. A) DGIM formation. B) Agarose gel electrophoresis of siRNA (500 ng) after incubation with different acylation reagents in ultrapure water at 37 °C for 4 h to form IM@RNA. The resulting complexes were purified using ice-cold ethanol. C) MALDI-TOF mass spectrum of cloaked siCOX1 with T2IM reagent. Peaks are assigned according to the number of TPP-acylated adducts, indicated in red. D) Uncloaking assay of IM@RNA under basic or reductive conditions. Samples were incubated for 24 h in 200 mM Tris buffer (pH 8.8) or with 20 mM GSH, followed by agarose gel electrophoresis. E) Evaluation of RNase A resistance for FAM-labelled acylated siRNA. PAGE analysis (FITC channel) of unmodified FAM-labelled siRNA and TPIM@siNC^{FAM} in the absence (-) or presence (+) of RNase A treatment. Lane marked (*) corresponds to free siRNA.

View Article Online
DOI: 10.1039/D6SC01497F

ARTICLE

Cellular Uptake and Mitochondrial Colocalization of IM@RNA

We next evaluated the cellular uptake and intracellular localization of IM-modified RNA (IM@RNA). Based on preliminary results indicating that effective cellular delivery occurred after 4 h, all subsequent experiments were performed using extended incubation times (Figure S5). Accordingly, HeLa cells were incubated with IM@siCOX1^{TMR} (100 nM, defined based on the siRNA concentration) for 48 h, followed by mitochondrial staining with MitoTracker Green and confocal microscopy analysis. As shown in Figure 3A, the control DGIM@siCOX1^{TMR} exhibited minimal overlap with mitochondrial signals, indicating inefficient mitochondrial localization. In contrast, as indicated by Pearson's correlation coefficients exceeding 0.75, TPP-containing IM@RNA constructs demonstrated pronounced colocalization with mitochondria (Figure 3A and 3B), confirming their effective transmembrane delivery into mitochondria. Similarly effective delivery was observed when siND1^{TMR} was administered to HepG2 cells, further confirming the generality of the mitochondrial targeting capability (Figure S6).

Furthermore, quantitative analysis corroborated these observations: flow cytometry revealed significantly higher fluorescence intensities for all TPP-linked IM@RNA samples compared with the DGIM control after 48 h of incubation (Figure 3C). These results confirm that incorporation of the TPP motif substantially enhances both cellular uptake and mitochondrial accumulation, consistent with its lipophilic and cationic properties that favor mitochondrial membrane permeation. Notably, linker architecture also influenced delivery efficiency. IM@RNA constructs bearing PEG-based linkers showed higher uptake efficiencies than TPIM, likely due to increased conformational flexibility and improved colloidal behavior, which may reduce nonspecific aggregation and lysosomal sequestration. To directly assess organelle specificity, cells were co-incubated with TEIM, T2IM, or the negative control DGIM and subjected to dual staining of lysosomes and mitochondria (Figures 3D and S7). Compared with DGIM, both TEIM and T2IM produced stronger intracellular signals and preferential co-localization with mitochondria, while showing minimal overlap with Lysotracker, indicating that the delivered siRNA largely avoided lysosomal capture. Collectively, these results confirmed that TPP-mediated reversible RNA acylation enables efficient cellular uptake and sustained mitochondrial localization, and insight that rational linker engineering provides an effective strategy to improve delivery efficiency and organelle specificity.

Mitochondrial Gene Silencing Efficiency of IM@RNA

Building on the validated mitochondrial delivery capability of the bifunctional IM@RNA platform, we next evaluated its ability to mediate functional gene silencing of mitochondria-encoded targets.[21,28] siRNAs against MTCO1 and MTND1, which encode key subunits of mitochondrial respiratory chain Complex IV and Complex I, respectively, were formulated into IM@RNA constructs. Cells were treated with IM@RNA formulations at a final concentration of 100 nM (based on the amount of siRNA, with each strand present at 100 nM), followed by Western blot (WB) analysis to assess target protein expression. Vinculin protein was used as reference loading control across all samples. Relative to the non-targeted control (DGIM@RNA), all TPP-conjugated IM@RNA formulations induced pronounced downregulation of their respective target proteins (Figure 4). Among them, TEIM@RNA and T2IM@RNA consistently exhibited superior silencing efficacy. For MTCO1, TEIM@siCOX1 achieved a knockdown efficiency of 60% ± 10%, while T2IM@siCOX1 resulted in more robust suppression, reaching 78% ± 15% (Figure 4A). Similarly, efficient silencing of MTND1 was observed across all TPP-linked constructs, with knockdown efficiencies exceeding 70%, and T2IM@siND1 displaying the strongest effect (Figure 4B). These trends closely mirror the mitochondrial targeting efficiencies observed in the imaging and flow cytometry analysis, underscoring the importance of effective mitochondrial localization for functional gene silencing.

We next investigated the temporal and concentration dependence of mitochondrial gene knockdown using TEIM@RNA and T2IM@RNA. Progressive reduction of target protein levels was observed with increasing incubation time, with pronounced knockdown occurring between 6 and 48 h (Figure 4C, 4D and S8). Dose-response studies were subsequently con-ducted by treating cells with IM@RNA at concentrations of 100, 50, 25, or 10 nM for 48 h. Both TEIM@RNA and T2IM@RNA exhibited clear concentration-dependent silencing behavior, with maximal knockdown at 100 nM and markedly reduced efficacy below 25 nM (Figure 4E). The specificity of mitochondrial gene silencing was further evaluated using T2IM@siND1. WB analysis revealed that knockdown was restricted to the intended target, with no detectable changes in the expression of Vinculin or MTCO1 across all tested concentrations (Figure 4F).

View Article Online
DOI: 10.1039/D6SC01497F

ARTICLE

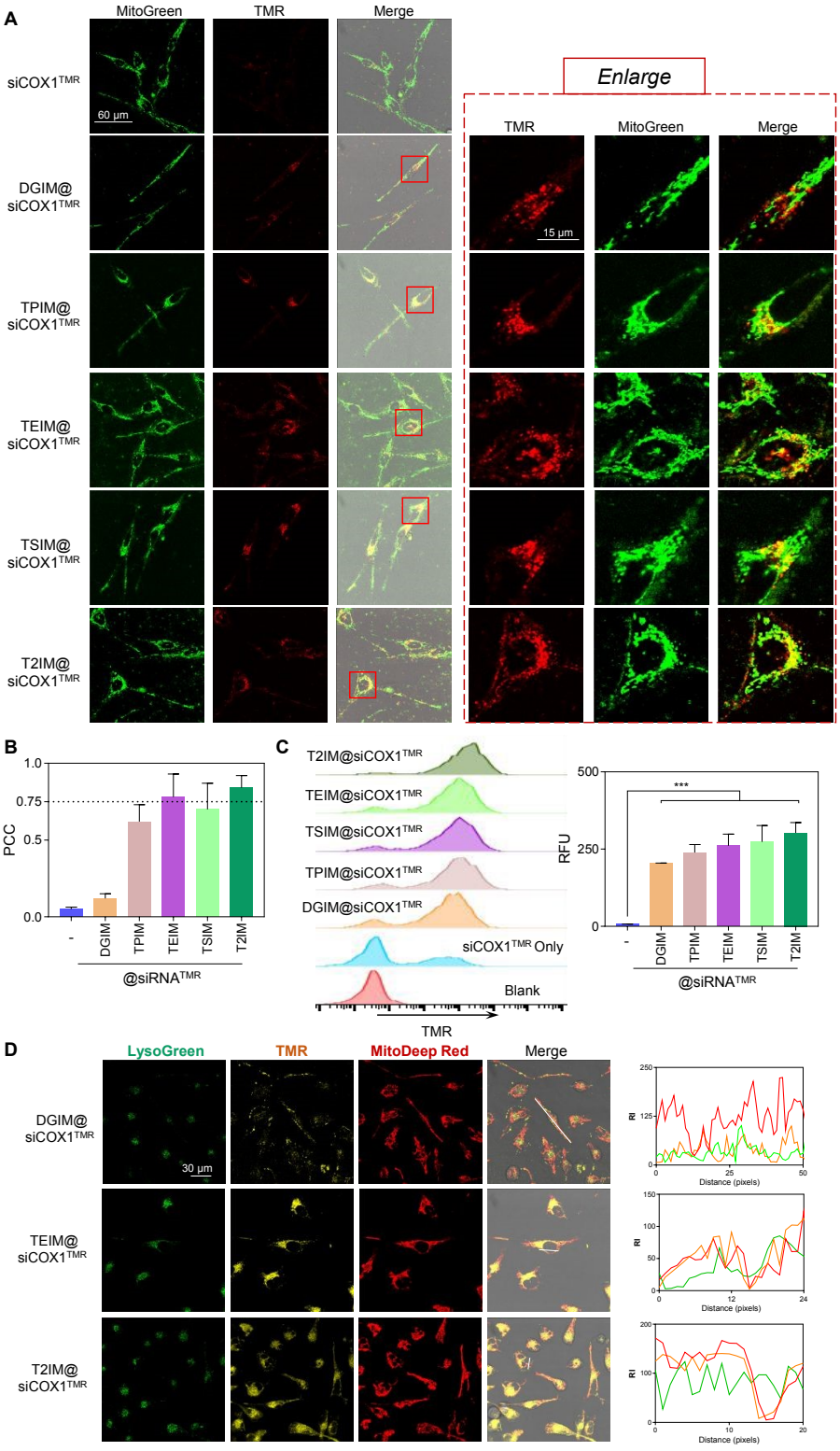

View Article Online DOI: 10.1039/D5SC04075

Figure 3 Cellular uptake and subcellular localization of TPP-acylated siCOX1 (TAMAR dye-labelled) complexes (IM@siCOX1^{TMR}). A) Confocal microscopy images showing cellular uptake and mitochondrial colocalization of IM@siCOX1^{TMR} (red channel). Cells were treated with 100 nM IM@siCOX1^{TMR} for 48 h, followed by staining with MitoTracker Green (mitochondria, green channel). The red boxes indicate regions enlarged in the panels to the right. B) Quantification of mitochondrial colocalization. The Pearson's correlation coefficient (PCC) between TMR and MitoTracker Green signals was calculated from confocal images (n=3 independent experiments). C) Flow cytometry analysis of cellular uptake. Cells treated with IM@siCOX1^{TMR} for 24 h were analyzed using the Cy3 channel. Histograms display the relative fluorescence intensity (RFU) of 10,000 cells per sample. Statistical significance was determined using one-way ANOVA with GraphPad Prism ***P < 0.001). D) Co-localization analysis of IM@siCOX1^{TMR} complexes (yellow channel) with mitochondria and lysosomes. Right plot: Quantitative fluorescence intensity profile analysis. ImageJ were used to extract and plot the fluorescence intensity along the line indicated in each channel.

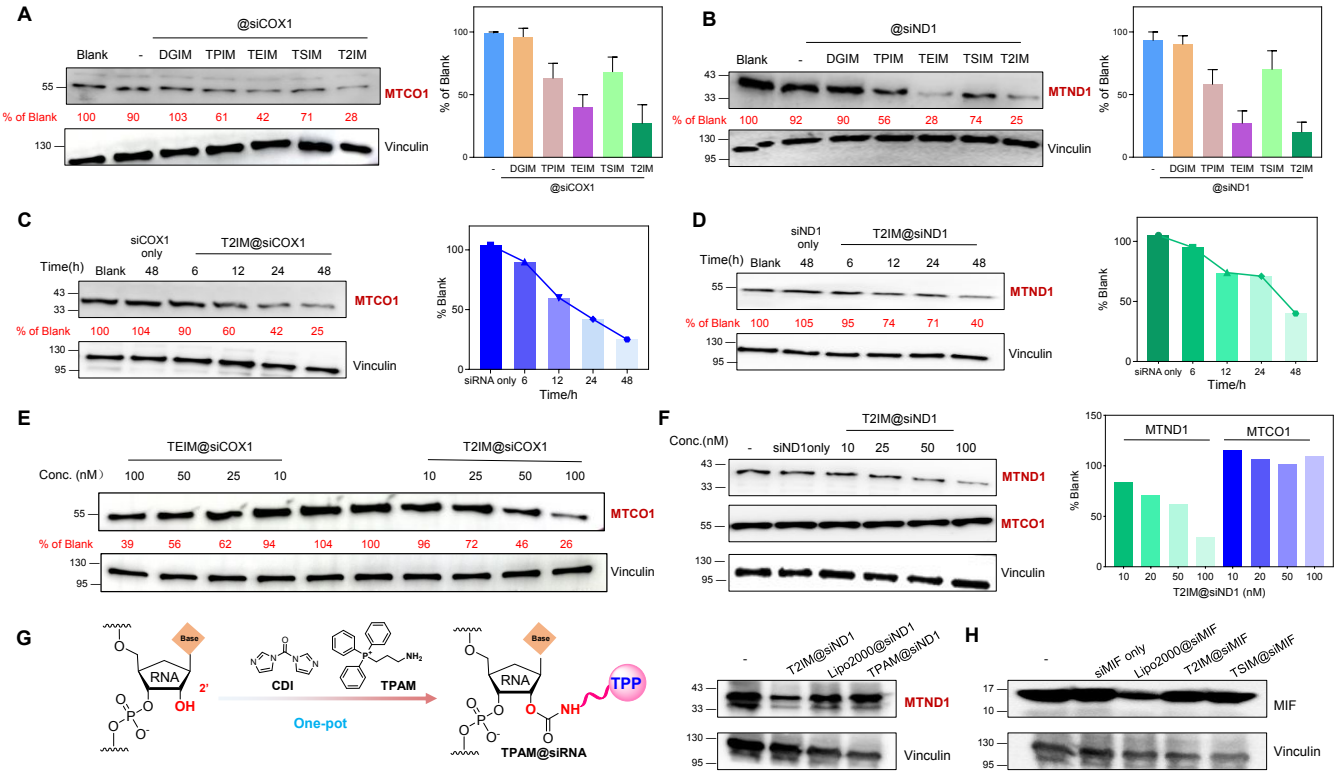

Figure 4 Targeted silencing of mitochondrial genes by TPP-acylated siRNA complexes. A) and B) Suppression of MTCO1 and MTND1 by different acylated complexes, respectively. Representative western blot and corresponding quantification of MTCO1\MTND1 protein levels in HeLa cells treated with 100 nM of the indicated IM@siND1 complexes for 48 h. C) and D) Time course of MTCO1 and MTND1 silencing, respectively. Representative western blot and quantification of MTCO1/MTND1 protein levels in HeLa cells treated with 100 nM T2IM@siCOX1 for the indicated durations. Blank: without any treatment. E) Dose-dependent silencing of MTCO1. Representative western blot of MTCO1 protein levels in HeLa cells treated for 48 h with TEIM@siCOX1 or T2IM@siCOX1 at the indicated concentrations. F) Dose-dependent silencing of MTND1. Representative western blot of MTND1 and MTCO1 protein levels in HeLa cells treated for 48 h with T2IM@siCOX1 at the indicated concentrations. Vinculin served as a loading control; treating with siRNA only (without any transfection reagent) served as a negative control. G) The formation of TPAM@RNA with a carbamate link. (Left) Sup-pression of MTND1 using T2IM, TPAM or lipo2000 reagents. (Right) H) Suppression of MIF protein using T2IM, TSIM or Lipo2000 reagents.

Moreover, to explore whether acylation can suppress siRNA activity and whether activity can be restored, we constructed control conjugates using triphenylphosphonium amine (TPAM, Figure 4G), which forms relatively stable carbonate linkages with RNA as reported by Kool and co-workers,[36] which is expected to be comparably irreversible under intracellular conditions. As shown in Figure 4G, we compared three conditions: (i) siRNA modified with non-cleavable TPP-NH2 (TPAM@siND1), (ii) siRNA delivered via Lipofectamine 2000 (Lipo2000@siND1), and (iii) our cleavable TPP-modified siRNA (T2IM@siND1). We observed that only the cleavable conjugate (T2IM@siND1) reduced MTND1 expression, where-as the non-cleavable TPP-modified siRNA (TPAM@siND1) showed minimal silencing activity. This suggests that permanent acylation masks siRNA function, and that restoration of activity requires cleavage of the linkage.

Further, to evaluate the role of mitochondrial targeting, we performed parallel experiments using siRNA against a cytosolic protein, MIF. Mitochondria-targeted constructs (T2IM@siMIF and TSIM@siMIF) showed significantly reduced knockdown efficiency compared to Lipo2000-delivered siMIF (Lipo2000@siMIF), which efficiently decreased cytosolic MIF levels (Figure 4H). This indicates that mitochondrial targeting restricts siRNA availability in the cytosol and is therefore critical for achieving selective knockdown of mitochondrial genes. Taken together, these results confirm that this platform enables time/dose-dependent, highly specific silencing of mitochondria-encoded genes without off-targets using reversible linkage chemistry.

Mitochondrial Functional Perturbation Induced by IM@siCOX1

Disruption of the mitochondrial respiratory chain is expected to induce pronounced functional and phenotypic alterations at the cellular level.[37-39] MTCO1 encodes a core subunit of respiratory Complex IV, whereas MTND1 encodes an essential subunit of Complex I (NADH: ubiquinone oxidoreductase) that is critical for its catalytic activity and proper assembly. Accordingly, silencing either gene is anticipated to directly impair oxidative phosphorylation. To assess the functional consequences of mitochondrial gene knockdown, we evaluated mitochondrial morphology, membrane potential (MMP), and reactive oxygen species (ROS) production.

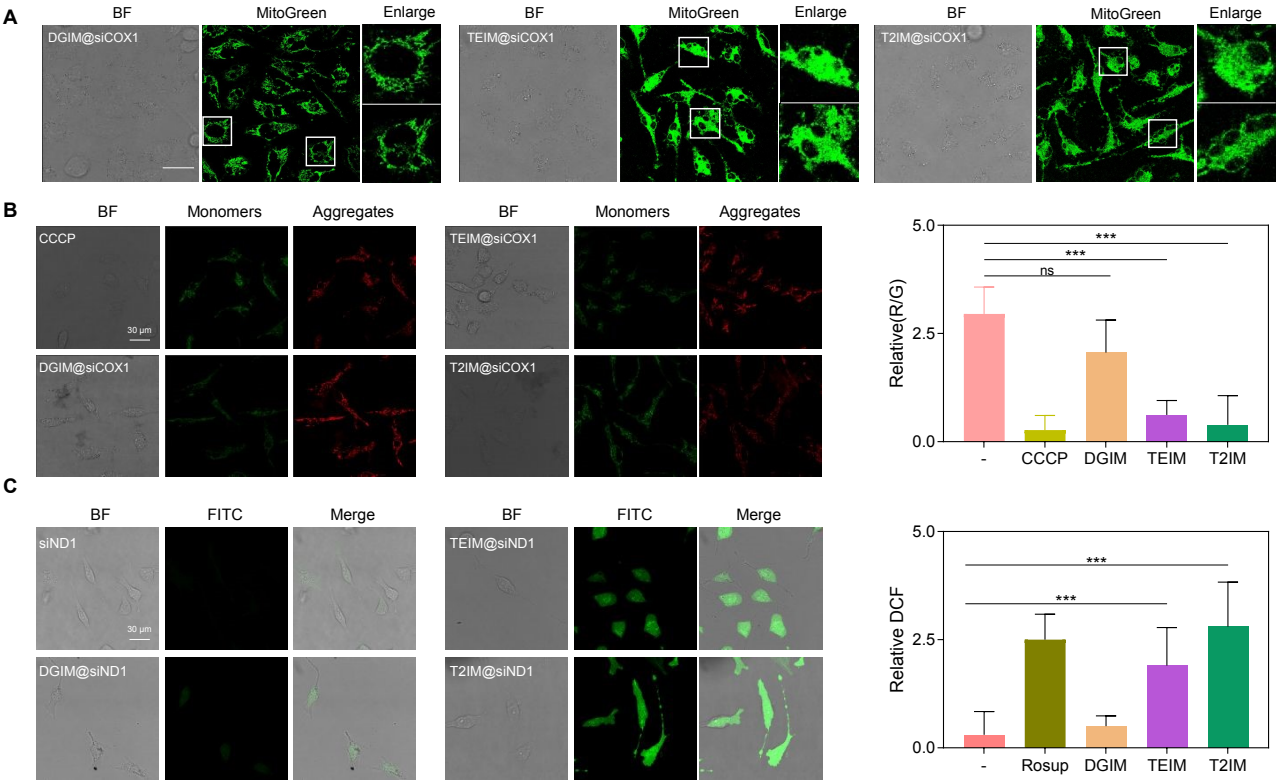

Figure 5 Assessment of mitochondrial function following mtDNA silencing by TPP-acylated siRNA. A) Morphological changes in mitochondria. Representative confocal microscopy images showing mitochondrial morphology in HeLa cells after 96 h of treatment with different IM@siCOX1 complexes (100 nM). Mitochondria were stained with MitoTracker Green (E_x/E_m: 490/516 nm). Scale bar: 20 μm. B) Detection of mitochondrial membrane potential ($\Delta\Psi_m$). JC-1 assay was performed on HeLa cells after treatment with different IM@siCOX1 complexes (100 nM, 48 h). CCCP-treated cells served as a positive control for depolarization. Fluorescence images show the distribution of JC-1 aggregates (red) and monomers (green), with the corresponding scatter plot showing the quantitative ratio of JC-1 aggregates to monomers (R/G) analyzed from confocal images using ImageJ. Data are presented as mean ± SD (n=3). Statistical significance was determined by one-way ANOVA (***P < 0.001, ns: not significant). C) Measurement of intracellular reactive oxygen species (ROS). DCFH-DA probe was used to measure ROS levels in HeLa cells treated with different IM@siND1 complexes (100 nM, 48 h). Flow cytometry histograms (FITC channel) show the distribution of DCF fluorescence intensity. The bar graph represents the relative mean fluorescence intensity (MFI) normalized to the control. Data are mean ± SD (n=3); statistical analysis as in B).

View Article Online
DOI: 10.1039/D6SC01497F

ARTICLE

HeLa cells were incubated with DGIM@siCOX1, TEIM@siCOX1, or T2IM@siCOX1 for 4 days, followed by staining with MitoTracker Green and confocal microscopy analysis. While overall cellular morphology remained comparable across all treatment groups, pronounced alterations in mitochondrial architecture were observed in the TPP-linked groups (Figure 5A). In the DGIM@siCOX1 control group, mitochondria retained an elongated, filamentous network. In contrast, mitochondria in TEIM@siCOX1-treated cells-and more prominently in T2IM@siCOX1-treated cells-displayed marked fragmentation and loss of filamentous structure (Figure 5A, enlarged views), a characteristic hallmark of mitochondrial dysfunction following MTCO1 depletion.[40,41] Consistent with these observations, migration assays revealed that TPP-linked groups exhibited reduced cell proliferation (Figure S9) and migratory capacity (Figure S10), reflecting compromised mitochondrial function and decreased cellular viability.

We next examined changes in mitochondrial membrane potential using the JC-1 probe. Cells treated with TEIM@siCOX1 or T2IM@siCOX1 (100 nM, 48 h) showed a substantial decrease in the red-to-green fluorescence intensity ratio compared with the Blank and DGIM@siCOX1 controls, indicating pronounced MMP depolarization (Figures 5B and S11A). Carbonyl cyanide m-chlorophenyl hydrazone (CCCP) served as a positive control. Notably, T2IM@siCOX1 induced the most severe reduction in MMP, approaching the level observed in CCCP-treated cells, thereby confirming effective disruption of mitochondrial respiratory function.

Mitochondrial dysfunction was further corroborated by analysis of intracellular ROS levels. Following 48 h incubation, cells stained with DCFH-DA exhibited markedly elevated ROS levels upon treatment with TEIM@siND1 and T2IM@siND1, as determined by confocal microscopy and flow cytometry (Figures 5C and S11B). ROS fluorescence intensities exceeded those observed for the positive control Rosup, whereas the non-targeted DGIM@siND1 group showed only minimal ROS elevation, indicating insufficient mitochondrial delivery. Taken together, these results show that TPP-mediated siRNA delivery operates effectively in cultured cells, producing robust mitochondrial gene silencing that translates into profound structural and functional mitochondrial changes.

In vivo Tumor Suppression by Mitochondria-Targeted IM@siND1

To extend our in vitro findings demonstrating that mitochondrial targeting of IM@RNA and modulation of mitochondrial genes (e.g., MTCO1 and MTND1) produced pronounced intracellular effects, we next evaluated the therapeutic potential of this strategy in vivo. Given the central role of mitochondrial dysfunction in tumor metabolism and proliferation, HepG2 cells were selected as a clinically relevant hepatocellular carcinoma model, and MTND1-a key subunit of mitochondrial respiratory Complex I-was chosen as the therapeutic target.[42,43]

A subcutaneous HepG2 xenograft model was established in nude mice to assess whether mitochondria-targeted IM@RNA-mediated MTND1 silencing could suppress tumor growth in vivo. Once tumors reached approximately 150 mm^3, mice were randomly assigned to three treatment groups: PBS, DGIM@siND1, or T2IM@siND1. Each group received daily intratumoral injections (1 μg of double-stranded siRNA per dose) for eight consecutive days (Figure 6A). As shown in Figure 6B, treatment with T2IM@siND1 led to pronounced tumor suppression after four injections, significantly slowing tumor growth and inducing progressive tumor regression. In contrast, tumors in the PBS and DGIM@siND1 groups continued to grow steadily. Quantitative analysis at the experimental endpoint revealed that T2IM@siND1 reduced tumor mass by approximately 60% relative to controls, whereas no statistically significant difference was observed between the PBS and DGIM groups (Figures 6C and 6D). Throughout the treatment period, all mice maintained stable body weights, indicating minimal systemic toxicity (Figure S12).

Mechanistic studies further confirmed effective and selective mitochondrial gene silencing in vivo. Western blotting and immunofluorescence analyses of tumor tissues showed that T2IM@siND1 selectively downregulated, MTND1 protein expression by 70-80% without affecting other mitochondrial proteins such as MTCO1 (Figures 6E, 6F, and S13). Functionally, MTND1 depletion is expected to disrupt electron transport chain activity, elevate ROS levels and trigger apoptosis. Consistent with this mechanism, TUNEL assays revealed extensive apoptotic signaling in tumors from the T2IM@siND1 group, where-as PBS- and DGIM-treated tumors exhibited minimal apoptosis (Figure 6G). Together, these results demonstrate that mito-chondria-targeted delivery of siND1 via T2IM enables potent and selective mitochondrial gene silencing in vivo, resulting in robust tumor suppression through apoptosis induction while maintaining favorable biocompatibility and minimal off-target effects.

View Article Online
DOI: 10.1039/D6SC01497F

ARTICLE

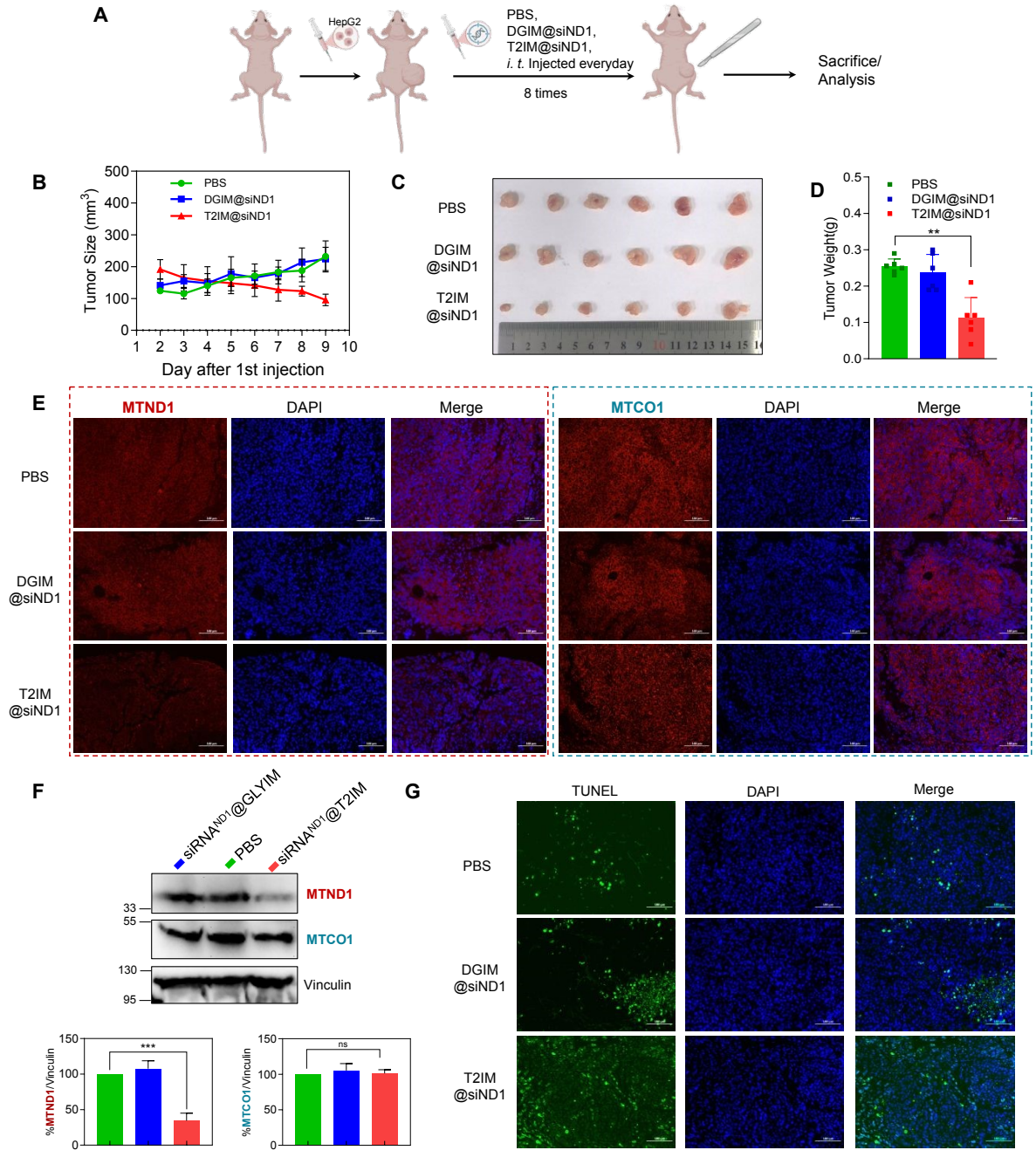

Figure 6 In vivo antitumor efficacy of mitochondria-targeting siRNA delivery in a mouse xenograft model. A) Schematic of the experi-mental design for tumor-bearing mouse treatment. Mice received daily intratumorally injections of either PBS, DGIM@RNA, or T2IM@RNA (1 μg RNA per mouse per day, n = 6). B) Tumor growth curve. Tumor volume was measured every day using a digital caliper and calculated by the formula: $V = L \times W^2 \times 0.52$, where L is tumor length and W is tumor width. Data are presented as mean ± SD (n=6 per group). C) Representative photographs of excised tumors from each treatment group at the endpoint. D) Quantification of tumor weight. Statistical significance was determined by one-way ANOVA **P < 0.01) (n=6). E) Immunofluorescence staining of MTND1 and MTCO1 in tumor tissues. F) Silencing of mitochondrial target proteins in tumor

View Article Online DOI: 10.1039/D5SC01497E

tissues. Representative western blot analysis and quantification (below) of MTCO1 and MTND1 protein expression in tumor lysates. Vinculin served as a loading control. Data are presented as mean ± SD (n=3). G) TUNEL staining and quantification of apoptotic cells within tumor tissues.

The simplicity, reversibility, and plug-and-play nature of this chemical platform distinguish it from existing mitochondrial delivery strategies that rely on permanent and structurally invasive modifications. Beyond its therapeutic potential, this approach provides a powerful tool for probing mitochondrial gene expression, protein biogenesis, and mitochondrial contributions to cellular physiology. Collectively, our results establish reversible 2'-OH RNA acylation as a versatile and translatable chemical framework for mitochondria-targeted RNA therapeutics and mitochondrial biology research

Conclusion

In summary, we have developed a chemically simple, modular, and user-friendly strategy for efficient RNA delivery to mitochondria and precise modulation of mitochondrial gene function in living cells and animals. By developing a TPP-conjugated, reversible 2'-OH acylation platform, we achieved transient RNA stabilization and mitochondrial targeting without permanently altering the RNA scaffold. Notably, this work represents the first demonstration of mitochondrial RNA delivery enabled by reversible DNA cloaking, highlighting the power of a single-step chemical modification to overcome longstanding delivery barriers. Using this platform, we achieved robust and selective silencing of mitochondria-encoded genes in cultured cancer cells, leading to pronounced mitochondrial dysfunction, elevated ROS production, and impaired cellular viability. Importantly, the same strategy translated effectively in vivo, where mitochondria-targeted delivery of siND1 significantly suppressed tumor growth in a xenograft model with minimal systemic toxicity and off-target effects.

Author contributions

Y. Zhuang: conceptualization, investigation, formal analysis, methodology, writing manuscript; X. Liu: Organic synthesis, invesitgation, formal analysis; Y. Shen: investigation, formal analysis; Q. Wang, Z. Lin, Q. Zeng and X. Chen: investigation and review; L. Jiang: supervision and funding acquisition; Shao Q. Yao: supervision, funding acquisition; J. Ge: conceptualization, resources, supervision, funding acquisition, writing manuscript.

Conflicts of interest

The authors declare that they have no competing interests.

Acknowledgements

We thank the National Natural Science Foundation of China (22377109, 22177104, 22505224), the Natural Science Foundation of Zhejiang Province (LR26B060003), the Fundamental Research Funds for the Provincial Universities of Zhejiang (RF-C2025005), National Medical Research Council (NMRC, 23-0740-A0001) and the Ministry of Education ((MOE, T2EP10222-0002) of Singapore for financial support.

Supplementary data

Supplementary data to this article can be found online at
Data availability

Notes and references

1 Burger, G.; Gray, M. W.; Lang, B. F. Mitochondrial genomes: anything goes. *Trends Genet.* 2003, **19**, 709-716.
2 Chen, X. J.; Butow, R. A. The organization and inheritance of the mitochondrial genome. *Nat. Rev. Genet.* 2005, **6**, 815-825.
3 Russell, O. M.; Gorman, G. S.; Lightowlers, R. N.; Turnbull, D. M. Mitochondrial Diseases: Hope for the Future. *Cell* 2020, **181**, 168-188.
4 Wen, H.; Deng, H.; Li, B.; Chen, J.; Zhu, J.; Zhang, X.; Yoshida, S.; Zhou, Y. Mitochondrial diseases: from molecular mechanisms to therapeutic advances. *Signal Transduct. Target. Ther.* 2025, **10**, 9.
5 Kopinski, P. K.; Singh, L. N.; Zhang, S.; et al. Mitochondrial DNA variation and cancer. *Nat. Rev. Cancer* 2021, **21**, 431-445.
6 Welch, D. R.; Foster, C.; Rigoutsos, I. Roles of mitochondrial genetics in cancer metastasis. *Trends Cancer* 2022, **8**, 1002-1018.
7 Wu, S. Y.; Lopez-Berestein, G.; Calin, G. A.; Sood, A. K. RNAi therapies: drugging the undruggable. Sci. Transl. Med. 2014, 6, 240ps7.
8 Wang, J. Y.; Doudna, J. A. CRISPR technology: A decade of genome editing is only the beginning. *Science* 2023, **379**, eadd8643.
9 Parhiz, H.; Atochina-Vasserman, E. N.; Weissman, D. mRNA-based therapeutics: looking beyond COVID-19 vaccines. *Lancet* 2024, **403**, 1192-1204.
10 Silva-Pinheiro, P.; Minczuk, M. The potential of mitochondrial genome engineering. *Nat. Rev. Genet.* 2022, **23**, 199-214.
11 Patananan, A. N.; Wu, T. H.; Chiou, P. Y.; Teitell, M. A. Modifying the Mitochondrial Genome. *Cell Metab.* 2016, **23**, 785-796.
12 Barrera-Paez, J. D.; Moraes, C. T. Mitochondrial genome engineering coming-of-age. *Trends Genet.* 2022, **38**, 869-880.
13 Li, N.; Wu, B.; Xiao, Y.; Hao, Y.; Wu, F.; Wei, Y.; Xu, Y.; Han, X. Tools and delivery technologies for mitochondrial gene editing. *Cell Biomater*. 2025, 100254.
14 Jiang, L.; Zhou, B.; Qian, H.; Wang, H.; Wang, Y.; Fan, W.; Zheng, G.; Ge, J. Cell-type-specific CRISPRization of mitochondrial DNA using bifunctional biodegradable silica nanoparticles. *Chem. Commun.* 2023, **59**, 9251-9254.
15 Liew, S. S.; Qin, X.; Zhou, J.; Li, L.; Huang, W.; Yao, S. Q. Smart Design of Nanomaterials for Mitochondria-Targeted Nanotherapeutics. *Angew. Chem. Int. Ed.* 2021, **60**, 2232-2256.
16 Zielonka, J.; Joseph, J.; Sikora, A.; Hardy, M.; Ouari, O.; Vasquez-Vivar, J.; Cheng, G.; Lopez, M.; Kalyanaraman, B. Mitochondria-Targeted Triphenylphosphonium-Based Compounds: Syntheses, Mechanisms of Action, and

Therapeutic and Diagnostic Applications. *Chem. Rev.* 2017, **117**, 10043-10120.
17 Cruz-Zaragoza, L. D.; Dennerlein, S.; Linden, A.; Yousefi, R.; Lavdovskaia, E.; Aich, A.; Falk, R. R.; Gomkale, R.; Schöndorf, T.; Bohnsack, M. T.; Richter-Dennerlein, R.; Urlaub, H.; Rehling, P. An in Vitro System to Silence Mitochondrial Gene Expression. *Cell* 2021, **184**, 5824-5837.
18 Cruz-Zaragoza, L. D.; Dahal, D.; Koschel, M.; Boshnakovska, A.; Zheenbekova, A.; Yilmaz, M.; Morgenstern, M.; Dohrke, J. N.; Bender, J.; Valpadashi, A.; Henningfeld, K. A.; Oeljeklaus, S.; Kremer, L. S.; Breuer, M.; Urbach, O.; Dennerlein, S.; Lidschreiber, M.; Jakobs, S.; Warscheid, B.; Rehling, P. Silencing mitochondrial gene expression in living cells. *Science* 2025, **389**, eadr3498.
19 Li, F.; Liu, Y.; Dong, Y.; Chu, Y.; Song, N.; Yang, D. Dynamic Assembly of DNA Nanostructures in Living Cells for Mitochondrial Interference. *J. Am. Chem. Soc.* 2022, **144**, 4667-4677.
20 Li, Y.; Li, J.; Chang, Y.; Zhang J.; Wang, Z.; Wang F.; Lin, Y.; Sui L. Mitochondria-targeted drug delivery system based on tetrahedral framework nucleic acids for bone regeneration under oxidative stress. *Chem. Eng. J.* 2024, **496**, 153723.
21 Gao, K.; Cheng, M.; Zuo, X.; Lin, J.; Hoogewijs, K.; Murphy, M. P.; Fu, X. D.; Zhang, X. *Cell Res.* 2021, **31**, 219-228.
22 Shi, Y.; Zhen, X.; Zhang, Y.; Li, Y.; Koo, S.; Saiding, Q.; Kong, N.; Liu, G.; Chen, W.; Tao, W. Chemically Modified Platforms for Better RNA Therapeutics. *Chem. Rev.* 2024, **124**, 929-1033.
23 Wang, Y.; Weissman, D.; Dong, Y. RNA chemistry and therapeutics. *Nat. Rev. Drug Discov.* 2025, **24**, 828-851.
24 Zhou, H.; Chen, D. S.; Hu, C. J.; Hong, X.; Shi, J.; Xiao, Y. Stimuli-Responsive Nanotechnology for RNA Delivery. *Adv. Sci.* 2023, **10**, e2303597.
25 Witten, J.; Hu, Y.; Langer, R.; Anderson, D. G. Recent advances in nanoparticulate RNA delivery systems. *Proc. Natl. Acad. Sci. U.S.A.* 2024, **121**, e2307798120.
26 Tang, Q.; Khvorova, A. RNAi-based drug design: considerations and future directions. N*at. Rev. Drug Discov.* 2024, **23**, 341-364.
27 Shaikh, A.; Neeli, P. K.; Singuru, G.; Panangipalli, S.; Banerjee, R.; Maddi, S. R.; Thennati, R.; Bathula, S. R.; Kotamraju, S. A functional and self-assembling octyl-phosphonium-tagged esculetin as an effective siRNA delivery agent. *Chem. Commun.* 2021, **57**, 12329-12332.
28 Lang, W.; Tan, W.; Zhou, B.; Zhuang, Y.; Zhang, B.; Jiang, L.; Yao, S. Q.; Ge, J. Mitochondria-Targeted Gene Silencing Facilitated by Mito-CPDs. *Chem. Eur. J.* 2023, **29**, e202204021.
29 Ali, L. M. A.; Su, D. D.; Mucci, R.; Martin, K.; Barboiu, M.; Lacour, J.; Bettache, N.; Ulrich, S. Mitochondria-Targeted Delivery of siRNA by Amphiphilic Nanovectors Self-Assembled from a Cationic [4]Helicene-Squalene Ester. *ChemBioChem* 2025, **26**, e202500537.
30 Xiao, L.; Fang, L.; Kool, E. T. 2'-OH as a universal handle for studying intracellular RNAs. Cell Chem. Biol. 2024, 31, 110-124.
31 Wang, S. R.; Wu, L. Y.; Huang, H. Y.; Xiong, W.; Liu, J.; Wei, L.; Yin, P.; Tian, T.; Zhou, X. Conditional control of RNA-guided nucleic acid cleavage and gene editing. *Nat. Commun.* 2020, **11**, 91.
32 Kohler, A.; Barrientos, A.; Fontanesi, F.; Ott, M. Kadina, A. M. Kietrys, E. T. Kool, RNA cloaking by reversible acylation. *Angew. Chem. Int. Ed.* 2018, **57**, 3059-3063.
33 Fang, L.; Xiao, L.; Jun, Y. W.; Onishi, Y.; Kool, E. T. Reversible 2'-OH acylation enhances RNA stability. *Nat. Chem.* 2023, **15**, 1296-1305.
34 Guo, J.; Chen, S.; Onishi, Y.; Shi, Q.; Song, Y.; Mei, H.; Chen, L.; Kool, E. T.; Zhu, R. Y. RNA control via redox-responsive acylation. *Angew. Chem. Int. Ed.* 2024, **63**, e202402178.
35 Lei, H.; Xiong, W.; Li, M.; Qi, Q.; Liu, X.; Wang, S.; Tian, T.; Zhou, X. Enhanced control of RNA modification and CRISPR-Cas activity through redox-triggered disulfide cleavage. *Bioorg. Med. Chem.* 2024, **112**, 117878.
36 Shioi, R.; Xiao, L.; Kool, E. T. Aqueous Activation of RNA 2'-OH for Conjugation with Amines and Thiols. *Bioconjugate Chem.* 2024, **35**, 40-50.
37 Gao, Y.; Sun, R.; Zhao, M.; Ding, J.; Wang, A.; Ye, S.; Zhang, Y.; Mao, Q.; Xie, W.; Ma, G.; Shi, H. On-Site-Specific Immobilization of Mitochondrial-Targeted NIR Fluorescent Probe for Prolonged Tumor Imaging. *Anal. Chem.* 2020, **92**, 6977-6983.
38 Zong, Y.; Li, H.; Liao, P.; Chen, L.; Pan, Y.; Zheng, Y.; Zhang, C.; Liu, D.; Zheng, M.; Gao, J. Mitochondrial dysfunction: mechanisms and advances in therapy. *Signal Transduc. t Target Ther.* 2024, **9**, 124.
39 Kohler, A.; Barrientos, A.; Fontanesi, F.; Ott, M. The functional significance of mitochondrial respiratory chain super complexes. *EMBO Rep.* 2023, **24**, e57092.
40 Zhai, R.; Fang, B.; Lai, Y.; Peng, B.; Bai, H.; Liu, X.; Li, L.; Huang, W. Small-molecule fluorogenic probes for mitochondrial nanoscale imaging. *Chem. Soc. Rev.* 2023, **52**, 942-972.
41 Ding, Y.; Li, J.; Zhang, J.; Li, P.; Bai, H.; Fang, B.; Fang, H.; Huang, K.; Wang, G.; Nowell, C. J.; Voelcker, N. H.; Peng, B.; Li, L.; Huang, W. Mitochondrial segmentation and function prediction in live-cell images with deep learning. *Nat. Commun.* 2025, **16**, 743.
42 Komza, M.; Chipuk, J. E. Mitochondrial metabolism: A moving target in hepatocellular carcinoma therapy. *J. Cell. Physiol.* 2025, **240**, e31441.
43 Kamalian, L.; Chadwick, A. E.; Bayliss, M.; French, N. S.; Monshouwer, M.; Snoeys, J.; Park, B. K. The utility of HepG2 cells to identify direct mitochondrial dysfunction in the absence of cell death. *Toxicol. in Vitro* 2015, **29**, 732-734.

View Article Online
DOI: 10.1039/D6SC01497F

The authors confirm that the data supporting the findings of this study are included within the article and its supplementary materials.